Scramjet Engine Model MASIV: Role of Mixing, Chemistry and Wave Interactions

Sean M. Torrez[*], James F. Driscoll[†], Derek J. Dalle[*],
Daniel J. Micka[*]

Dept. of Aerospace Engineering, University of Michigan, Ann Arbor MI 48109

Presented at the AIAA Joint Propulsion Conference, Denver, Colorado, August 2009

This paper provides details of the combustion and inlet submodels used in the Michigan-Air Force Scramjet In Vehicle (MASIV) model. The model solves conservation equations in 1-D, using several modeling techniques to retain some of the fidelity of higher-order simulations. Inlet wave interactions, fuel mixing and finite-rate chemistry are considered. The order of the problem is reduced by physics-based, experimentally-verified algebraic scaling laws, which retains the required physics but reduces the computation time of the problem to seconds, instead of the several days required by computational fluid dynamics (CFD). Scaling coefficients and assumptions are given. The model is used to compute the performance of an experimental configuration for which real data are available.

I.   Introduction

Since CFD codes take a long time to reach solutions for reacting ducts, a tool that can solve these configurations in short time to acceptable accuracy is highly desirable for control and design applications. The MASIV code [1, 2] seeks to solve for the heat release distribution in ramjet and scramjet combustors, which is used to compute the thrust of hypersonic vehicle engines. Since finite-rate chemistry is highly dependent on the temperature and pressure in the combustor, MASIV also uses an inlet wave interaction technique to predict the effects of the wave interactions that occur in the vehicle inlet.

There are two components to the current generation of MASIV: an inlet code which computes wave interactions for arbitrarily shaped bodies and a combustor code which computes supersonic combustion in arbitrarily shaped ducts with jet fuel injection. The inlet model solves a series of exact Riemann[3] problems between any two adjacent regions. This gives the classical inviscid solution to any two-wave interaction problem. The model considers shock-shock, shock-expansion and expansion-expansion interactions, modeling expansions as a series of discrete waves.

The combustor code solves a set of differential and algebraic equations in space,[4] marching axially through the combustion duct. Since combustion in most engines is mixing-limited rather than reaction rate-limited, jet mixing is computed using the scaling law of Hasselbrink and Mungal,[5] which is based on flow field similarity. The model considers finite-rate chemistry via the Stationary Laminar Flamelet Model (SLFM),[6] which considers each point in the flame and maps it to the solution of a corresponding counter-flow flamelet. Because this is a Probability Distribution Function approach, it includes the effects of different strain fields, species diffusion, and momentum diffusion as the duct velocity and fuel jet velocity change.

In this study, we compare results from experiments done at the University of Michigan to results generated by the MASIV code. MASIV is intended to solve duct combustion problems in short time relative to computational fluid dynamics. Although it can solve for the flow through arbitrary ducts, this effort concentrates on combustion modeling for hypersonic vehicle engine (i.e., ramjet and scramject engines). Therefore, we compare the model to experiments done on the dual-mode combustor at the University of Michigan, and the station numbering is that of the generic hypersonic vehicle shown in Figure 1.

---

[*]Research Assistant, Student Member, AIAA
[†]Professor of Aerospace Engineering, Fellow, AIAA

Stations:

Ⓡ︎   -   Free stream conditions

(1a)
(1b)   }   After each inlet vertex
⋮

(2a)   -   After diffuser
(3a)   -   After isolator

(4a)
(4b)   }   After each significant change in the combustion duct (injectors, area changes)
⋮

(5a)   -   After combustor (beginning of nozzle)
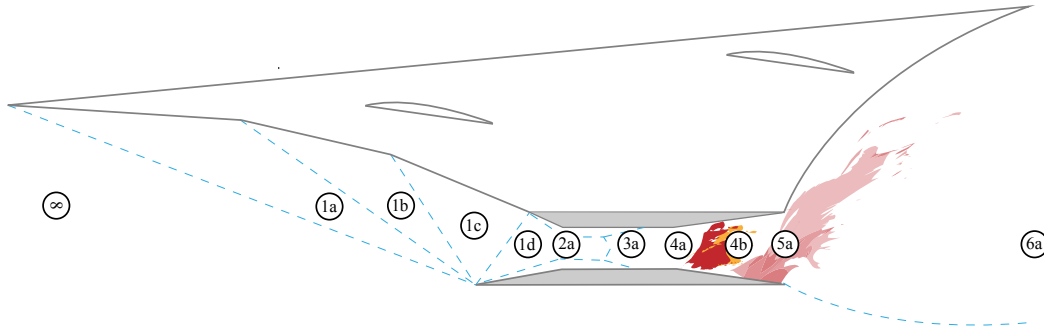(6a)   -   After external nozzle (end of engine)

Figure 1. An example geometry. The station numbers are extensible by adding successive letters to each station for a more complex geometry.

II. Inlet model

We consider a scramjet inlet design that is approximately two-dimensional. A satisfactory control-oriented model must require a relatively small amount of computational time and still yield a relatively accurate solution for the inlet flow. Instead of solving directly for the flow conditions at each point in the flow (as is done in CFD), the proposed method solves for the positions of the relevant waves, which separate regions in which the flow properties are considered to be uniform. The inlet-modeling method solves for the locations of the shock waves and expansions using established two-dimensional supersonic theory. To make this possible in a digital computing environment, expansion fans are approximated as a number of discrete isentropic waves. In many ways this is a generalized and automated version of the method of characteristics.

A. Description of the Proposed Algorithm

The input to the program consists of two parts. The first input is the geometry of the inlet, which consists of two polygons: one for the main body of the vehicle and one for the cowl. The second part of the input is the flight conditions, *i.e.* M_∞, α, and altitude. The program begins its analysis slightly upstream of the leading edge and marches toward the downstream x-coordinate, x_{2a}. As the program proceeds downstream, it tracks the positions of all the straight lines in the flow, which includes waves, the surfaces of the input geometry, and the boundaries of the flow domain. Within the program each of these straight lines is tracked as a path that consists of a point and a propagation angle.

As the model is computing the flow solution, there is a current x-coordinate. Call this value x_{cur}. This creates a vertical line $x = x_{cur}$ for which all of the flow upstream has been computed, and all of the flow downstream remains to be solved. There will be several paths that intersect this vertical line at vertical coordinates of $z_1, z_2, \ldots$, each path having a corresponding propagation angle of $\sigma_1, \sigma_2, \ldots$. Then two paths

American Institute of Aeronautics and Astronautics

with coordinates z_j and z_{j+1} have a downstream intersection point of

$$x_{\text{next},j} = x_{\text{cur}} + \frac{z_{j+1} - z_j}{\tan \sigma_{j+1} - \tan \sigma_j} \tag{1}$$

provided that $\sigma_j < \sigma_{j+1}$. Then the x-coordinate of the next interaction point, x_{next}, is the minimum of all the $x_{\text{next},j}$ and all of the vertices of the input polygons that are downstream of x_{cur}.

Once an interaction point is found, the nature of the interaction is determined, and the local flow problem is solved. If one of the paths is a surface boundary, the program determines the downstream conditions using either a shock or expansion that turns the flow parallel to the surface. If all of the interacting paths are waves, the solution is determined by a Riemann problem, which is described in Section II.C. Before moving to the next interaction point, the list of waves and their propagation angles at the current x-coordinate are updated so that the coordinates of the next interaction point can be determined. This inlet model will provide a flow solution in less than ten seconds for all of the flight conditions considered in this report.

B. Discretized Prandtl-Meyer Expansions

The Prandtl-Meyer theory for expansions is used to predict the solution for a supersonic flow turned away from itself. In addition to determining the conditions downstream, Prandtl-Meyer theory predicts the conditions along the characteristics within the expansion fan. The geometry of this situation is illustrated in Fig. 2.

a) Geometry and definitions   **b)** Example
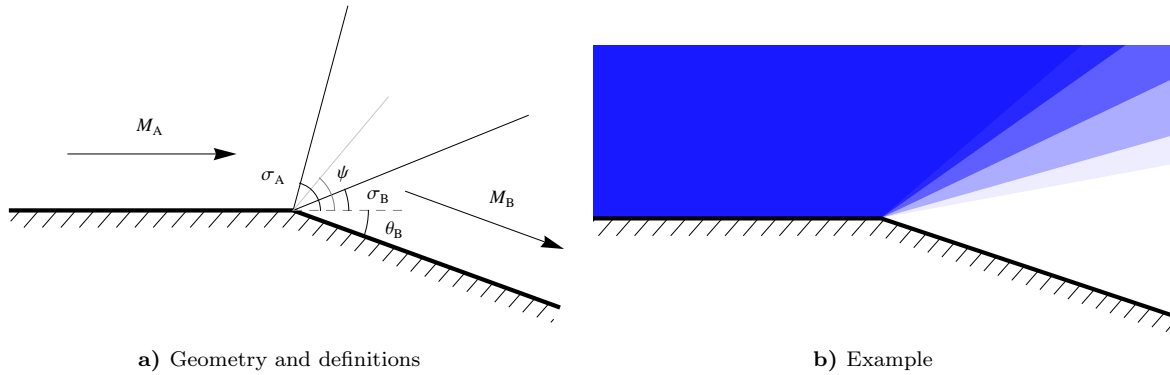
Figure 2. Illustration of Prandtl-Meyer expansion wave. The geometry and nomenclature of the problem are shown 2a) while 2b) shows an example solution from the proposed inlet model in which the expansion fan is modeled as five discrete waves. Darker shades of blue represent higher pressures.

Assuming $\theta_B < \theta_A$, the conditions downstream of a two-dimensional expansion can be found using the characteristic equation $\nu_B + \theta_B = \nu_A + \theta_A$ where ν is the Prandtl-Meyer angle. The angle of the first characteristic is $\sigma_A = \theta_A + \mu_A$, and the last characteristic has an angle of $\sigma_B = \theta_B + \mu_B$ where $\mu = \sin^{-1} 1/M$ is the Mach angle. However, this does not resolve the flow between the first and last characteristics. To find the Mach number along a characteristic whose angle with the freestream velocity is ψ, the characteristic equation is

$$\psi = \nu_A + \theta_A + \mu(\psi) - \nu(\psi) \tag{2}$$

For a calorically perfect gas, this equation has an explicit solution;

$$M = \sqrt{1 + \frac{\gamma + 1}{\gamma - 1} \tan^2 \left(\sqrt{\frac{\gamma - 1}{\gamma + 1}} \left(\nu_A + \theta_A - \psi + \frac{\pi}{2} \right) \right)} \tag{3}$$

The resolution within the expansion wave, given in equation (3) provides a method to discretize the wave. By selecting a set of angles for evaluation $\psi_1, \ldots, \psi_{n_{\text{ex}}}$ between σ_B and σ_A, the expansion can be split into a set of regions within which the gas properties are constant. The regions are separated by discrete waves, which have angles of $\sigma_1, \ldots, \sigma_{n_{\text{ex}}}$. Once the evaluation angles, $\psi_1, \ldots, \psi_{n_{\text{ex}}}$, have been selected, the intermediate Mach numbers, $M_1, \ldots, M_{n_{\text{ex}}}$, are calculated using equation (3). Finally, we select wave angles that conserve mass flux through the expansion wave.

C. Two-dimensional Riemann Problem

A two-dimensional Riemann problem describes the situation in steady two-dimensional compressible flow in which two uniform regions are in contact with each other, *e.g.* at the trailing edge of an airfoil or the intersection of two oblique shocks. At the point of interaction, there are two inconsistent flow conditions. To rectify this situation, the gas in both regions must pass through a wave, as shown in Figure 3.
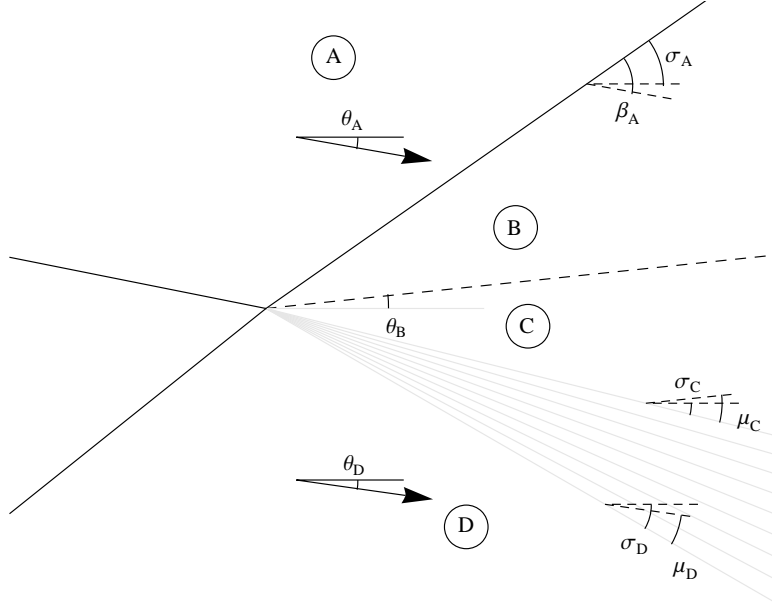

Figure 3. Geometry for the interaction between two waves with a Riemann problem whose solution has a shock and an expansion. In the general Riemann problem, both waves could be either a shock or an expansion.

The physical solution must have the property that the intermediate regions B and C must have equal pressures and flow in the same direction. Thus $p_B = p_C$ and $\theta_B = \theta_C$. A simple solution method is to define a single pressure-deflection function

$$p_B = p(A, \theta_B - \theta_A) \tag{4}$$

which takes as input all information about state A and a deflection angle $\theta_B - \theta_A$, and returns a post-wave pressure as output. If $\theta_B < \theta_A$, the Prandtl-Meyer expansion relations are used, while if $\theta_B > \theta_A$, the oblique shock relations are used. Using the same pressure-deflection for the lower angle and applying the constraints gives

$$p(A, \theta_B - \theta_A) = p(D, \theta_D - \theta_B) \tag{5}$$

which is satisfied only by the correct value of θ_B.

D. Downstream Averaging Model

At the downstream boundary of the reference inlet geometry, it is useful to define the spatially averaged gas properties, which can be input into a one-dimensional isolator or combustor model. With the proposed inlet model, gas properties are not uniform at the downstream boundary of the inlet because of the possible presence of waves separating regions of different gas properties. The proposed method to determine spatially-averaged properties is to require that the total fluxes of mass, momentum, and stagnation enthalpy are constant through the $x = x_{2a}$ plane. This method is chosen so that the averaging does not violate conservation of mass or energy and introduces no drag. The geometry of this scheme is shown in Figure 4.

The mass flux out of the averaging plane is

$$\Phi_\rho = \rho_2 u_2 H_2, \tag{6}$$

and the mass flux into the averaging plane is

$$\Phi_\rho = \sum_{i=1}^{n_2} \rho_{1k_i} u_{1k_i} H_{1k_i} \cos \theta_{1k_i} \tag{7}$$

American Institute of Aeronautics and Astronautics

where H_{1k_i} is the height of region $1k_i$ at its downstream edge. We use the same process to determine the momentum flux out of the inlet, $\Phi_u = \rho_2 u_2^2 H_2$, and the stagnation enthalpy flux, $\Phi_h = \rho_2 u_2 H_2 h_{0,2}$.

Once the fluxes into the averaging plane have been calculated, the state variables for the flow out of the inlet can be determined. The isolator velocity is $u_2 = \Phi_u/\Phi_\rho$, the stagnation enthalpy is $h_{0,2} = \Phi_h/\Phi_\rho$, and the density is $\rho_2 = \Phi_\rho/(u_2 H_2)$. The pressure and temperature at station 2 are determined using an equation of state.
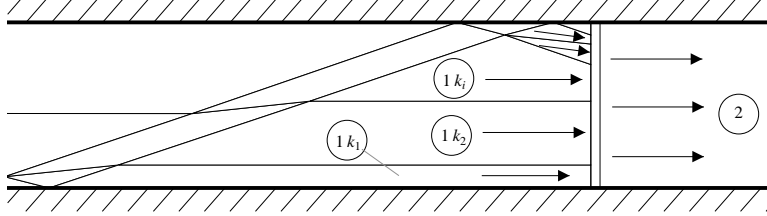

Figure 4. This figure shows the averaging plane at the downstream end of the inlet. The thin black lines represent waves from a sample inlet solution. Region $1k_1$ is the lowest region that has a boundary along the averaging plane; region $1k_2$ is the region above that; *etc.* In this example there are $n_2 = 6$ regions that contact the averaging plane.

E. Comparison to CFD

We consider an example scramjet inlet geometry to validate the proposed inlet model. The geometry has exactly four shocks and no spillage for a flight Mach number of $M_\infty = 8.0$ and angle of attack of $\alpha = 0$ assuming sharp-nosed leading edges and an inviscid, calorically perfect (constant c_p) flow. The first three shocks are generated by external ramps, and they turn the flow away from the center of the vehicle. The fourth shock turns the flow back to horizontal, and it intersects the shoulder in the upper surface of the inlet. Therefore there are no additional shocks downstream of this fourth shock. Under these flight conditions, the compression ratio of the inlet is $p_2/p_\infty = 30.61$, and the pressure recovery factor is $p_{0,2}/p_{0,\infty} = 0.6841$.

When this inlet is operated at off-design Mach numbers or angles of attack, additional waves are formed. To compare the results of the proposed inlet model to a high-fidelity two-dimensional CFD solution, we selected a flight condition of $M_\infty = 10.0$ and $\alpha = 0$. The results of the two computations are shown in Figure 5. The two predicted flow solutions look very similar, and to quantify this similarity, Figure 6 shows the pressure along the downstream boundary ($x = x_{2a}$). The two results have the same trend, and the spatially averaged pressure, p_2, is accurate to within 2.0%. The other spatially averaged thermodynamic variables, ρ_2, T_2, and u_2, are even more accurate. As a result of this comparison, we expect that the proposed inlet model can be expected to predict the thermodynamic properties to within 10% for a wide range of flight conditions.

III. Combustion Modeling

The MASIV code marches the flow conservation equations from the beginning of the combustor (station 3a) to the end of the internal nozzle (station 5a). All flow states are allowed to vary in the downstream axial direction, defined $-\hat{x}$. We allow derivatives with respect to the axial coordinate only. Some quantities, such as jet spreading and mixing, vary in the transverse directions, but they may only vary algebraically, such that their evolutions do not depend on the information propogating downstream.

A. Duct Solution

We begin with the conservation equations, along with the equation of state.

We take the derivatives of these equations with respect to x to obtain a set of ODEs, which are presented in Table 2. These equations form the basis of the model, since their simultaneous solution provides all the information needed to calculate the evolutions of the state variables (p, ρ, T) and the heat release through the duct.

American Institute of Aeronautics and Astronautics

a) Proposed model solution
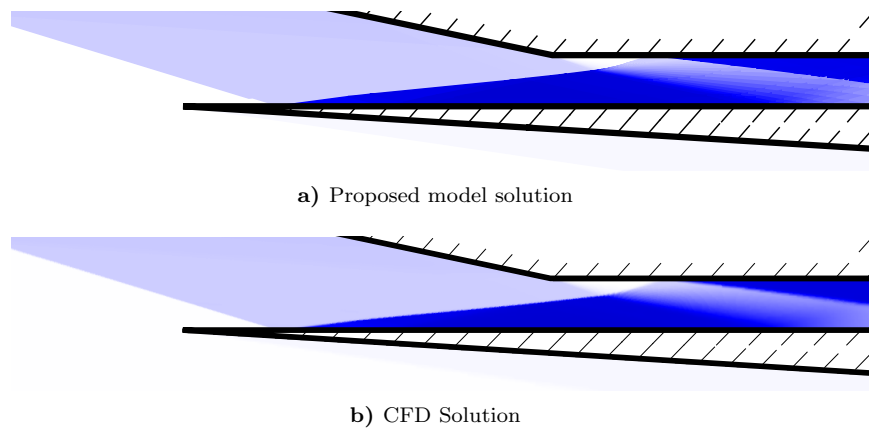

b) CFD Solution

Figure 5. Comparison between solution from proposed inlet model and high-fidelity CFD solution. Darker shades of blue represent regions of higher pressure; white represents freestream pressure and black represents $p/p_\infty = 90$.
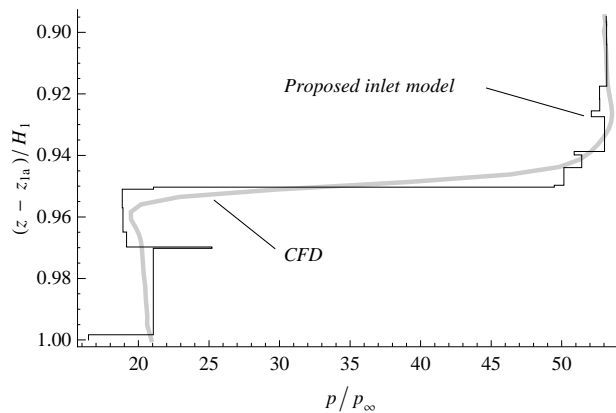

Figure 6. The normalized pressure along the z-axis of the inlet outflow plane is shown for both the proposed inlet model and the two-dimensional CFD result.

Table 1. Conservation equations used in MASIV.

Equation Name	Equation
Equation of State	$p = \rho \frac{\mathcal{R}}{W} T$
Cons. of Mass	$\frac{\partial}{\partial t} \iiint_V \rho dV + \iint_S \rho \vec{u} \cdot \vec{n} dS = 0$
Conservation of Species	$\frac{\partial}{\partial t} \iiint_V Y_i \rho dV + \iint_S Y_i \rho \vec{u} \cdot \vec{n} dS = \dot{\omega}$
Cons. of Momentum	$\frac{d}{dt} \iiint_V \rho \vec{u} dV = - \iint_S (\rho \vec{u}) \vec{u} \cdot \vec{n} dS + \iiint_V \rho \vec{f} dV + \iint_S \bar{\bar{\sigma}} \vec{n} dS$
Cons. of Energy	$\frac{d}{dt} \iiint_V \rho (e + \frac{\vec{u} \cdot \vec{u}}{2}) dV + \iint_S \rho (e + \frac{\vec{u} \cdot \vec{u}}{2}) \vec{u} \cdot \vec{n} dS + \iint_S p \vec{u} \cdot n dS = \iiint_V \rho \vec{f} \cdot \vec{u} dV + \dot{Q} + \dot{W}$

Since the specific heat capacity, c_p of each species varies with T, which varies through the duct, using c_p to calculate enthalpy offers no advantage, so we avoid formulating the problem in this way. The JANAF and GRIMech tables are readily available (CHEMKIN[7] is one convenient source), so we simply use the enthalpy (h) curve fits, and circumvent a messy formulation for c_p. If the specific heat is desired, it can be computed *a posteriori*.

Similarly, the sound speed (a) for a reacting flow is not defined $a = \sqrt{\gamma R T}$, but instead must be defined as $a = (\frac{\partial p}{\partial \rho})_{s=const.}$. We avoid this difficulty by formulation the problem in terms of velocity rather than Mach number. This is what Heiser and Pratt[8] call enthalpy-kinetic energy (H-K) space. It is more convenient than the typical temperature-Mach number (T-M) space, giving a simpler set of equations. If desired, a and M can be computed post-solution as well as c_p.

Table 2. Differential equations used in MASIV.

ODE Name	Equation
Equation of State	$\frac{1}{p}\frac{dp}{dx} = \frac{1}{T}\frac{dT}{dx} + \frac{1}{\rho}\frac{d\rho}{dx} - \frac{1}{W}\frac{dW}{dx}$
Cons. of Mass	$\frac{1}{\rho}\frac{d\rho}{dx} = \frac{1}{\dot{m}}\frac{d\dot{m}}{dx} - \frac{1}{u}\frac{du}{dx} - \frac{1}{A}\frac{dA}{dx}$
Cons. of Species	$\frac{dY_i}{dx} = \frac{\dot{\omega}}{\rho u} + \frac{1}{\dot{m}}\frac{d\dot{m}_i}{dx} - \frac{Y_i}{\dot{m}}\frac{d\dot{m}}{dx}$
Cons. of Momentum	$\frac{1}{u}\frac{du}{dx} = -\frac{1}{\rho u^2}\frac{dp}{dx} - \frac{C_f}{2A}\frac{dS_w}{dx} - \frac{(1-\varepsilon)}{\dot{m}}\frac{d\dot{m}}{dx}$
Cons. of Energy	$\frac{1}{h_0}\frac{dT}{dx}\sum_i c_{p,i} Y_i = -\frac{u}{h_0}\frac{du}{dx} - \frac{1}{\dot{m}}\frac{d\dot{m}}{dx} + \frac{1}{h_0 \dot{m}}\frac{\rho u C_f (h_{aw}-h_w)}{2Pr^{2/3}}\frac{dS_w}{dx} \cdots$ $+ \frac{1}{h_0 \dot{m}}\frac{\rho u^3 C_f}{2}\frac{dS_w}{dx} - \frac{1}{h_0}\sum_i h_i \frac{dY_i}{dx} + \frac{1}{h_0 \dot{m}}\sum_i h_i \frac{d\dot{m}_i}{dx}$

Clearly, there are several other quantities indicated in Table 2 which are required to solve the system, but which are not part of the solution. These are presented in Table 3.

B. Chemistry

We compute the reaction rate ($\widetilde{\omega}_i$) for each species using the SLFM before solving the set of ODEs.[9] The SLFM uses a counter-flow flamelet solution with an assumed PDF model for each flow parameter: mean mixture fraction ($\tilde{f}$), mean mixture fraction variance ($\widetilde{f'}$) and mean scalar dissipation rate ($\widetilde{\chi}$). This means that for any given point in the flow, $\widetilde{\omega}_i$ can be determined as a function of $\tilde{f}$, $\widetilde{f'}$ and $\widetilde{\chi}$. The SLFM equation follows.

$$-\chi_{st}\frac{\partial \boldsymbol{\psi}}{\partial f} = \frac{\dot{\mathbf{m}}}{\rho} \tag{8}$$

Here, $\boldsymbol{\psi}$ and $\dot{\mathbf{m}}$ represent the vectors

Table 3. Additional equations used in MASIV.

Source	Variable	Equation
From Solution	p	$= \int \frac{dp}{dx} dx$
	ρ	$= \int \frac{d\rho}{dx} dx$
	Y_i	$= \int \frac{dY_i}{dx} dx$
	u	$= \int \frac{du}{dx} dx$
	T	$= \int \frac{dT}{dx} dx$
Given	A	$= A(x)$
	$\frac{dA}{dx}$	$= \frac{dA}{dx}(x)$
	$\frac{d\dot{m}_i}{dx}$	$= \frac{d\dot{m}_i}{dx}(x)$
	$\dot{\omega}$	$= \dot{\omega}(x)$
	W_i	$= const.^{\dagger}$
	C_f	$= const.$
Computed	$\dot{m}$	$= \rho u A$
	$\frac{dW}{dx}$	$= -W^2 \sum_i \left(\frac{1}{W_i} \frac{dY_i}{dx} \right)$
	$\frac{dS_w}{dx}$	$= \sqrt{16A + \left(\frac{dA}{dx}\right)^2}$
	$\frac{d\dot{m}}{dx}$	$= \sum_i \frac{d\dot{m}_i}{dx}$
	h_i	$= h_i(T)^{\dagger}$
	h	$= \sum_i h_i$
	h_0	$= h + \frac{u^2}{2}$
	h_w	$= h(T_w)$
	h_{aw}	$= h + \sqrt{\text{Pr}} \frac{u^2}{2}$

†from CHEMKIN

$$
\boldsymbol{\psi} = \begin{bmatrix} Y_1 \\ \vdots \\ Y_n \\ h \end{bmatrix}
\qquad\qquad
\dot{\mathbf{m}} = \begin{bmatrix} \rho\dot{\boldsymbol{\omega}}_1 \\ \vdots \\ \rho\dot{\boldsymbol{\omega}}_n \\ -\dot{q}_R \end{bmatrix}
\tag{9}
$$

This results in a flamelet lookup table of reaction rates for each species, $\dot{\mathbf{m}}(f, \chi_{st})$. The solution of the flamelet equations has been discussed sufficiently in the literature (see [6]), so discussion will be omitted here.

Once a flamelet solution has been found, we require mean values of each variable in order to use the mixing model discussed in Section C. This is accomplished using a probability density function approach which assumes a certain PDF and variance for each quantity, then integrates the product over the parameter space.

For example, to compute the mean of the reaction source terms, which we desire as reaction rate input into the duct solution code, the following equation applies.

$$
\widetilde{\dot{\mathbf{m}}}(\tilde{f}, \widetilde{f''^2}, \bar{\chi}_{st}) = \int_0^{\infty} \int_0^1 \dot{\mathbf{m}}(f, \chi_{st}) \widetilde{P}(f) P(\chi_{st}) df\, d\chi_{st}
\tag{10}
$$

where $\widetilde{P}(f)$ is the beta PDF, $\beta(f, \tilde{f}, \widetilde{f''^2})$ and $P(\chi_{st})$ is a log-normal PDF. Finally, a mapping from $\widetilde{\chi}$ to $\bar{\chi}_{st}$

is required, which can be accomplished using another PDF

$$\widetilde{\chi} = \bar{\chi}_{st} \int_0^1 F(f) \beta(f, \tilde{f}, \widetilde{f''^2}) df \tag{11}$$

These functions are tabulated for a given chemistry to improve solution speed. In principle, it is possible to pre-tabulate chemistry for any given configuration. In application, it is best to use a limited number of chemistry files in order to reduce the amount of memory and disk space required.

C.   Assumed Mixing Model

The jet centerline penetration and spreading can be computed for each point using the scaling relationship measured in [10]. This relationship is valid for momentum ratio $r_u \gg 1$. Experimental results set the values of the constants in Table 4, which allow MASIV to generate a predicted three-dimensional distribution of fuel based on injection and crossflow parameters.

First, the momentum ratio is defined as

$$r_u = \left[\frac{\rho_{inj}}{\rho} \left(\frac{u_{inj}}{u} \right)^2 \right]^{1/2} \tag{12}$$

which appears in the scaling relationship

$$\frac{y_{CL}}{d_{inj}} = c_1 \left(\frac{x_{CL}}{d_{inj}} \right)^{c_2} r_u^{2/3} \tag{13}$$

to trace the centerline path of the fuel jet.

The normalized concentration of injected fuel is given by another scaling relationship:

$$\frac{C_{CL}}{C_{inj}} = c_3 \left(\frac{\rho_{inj}}{\rho} \right)^{1/3} \left(\frac{u_{inj}}{u} \right)^{-1/3} \left(\frac{x_{CL}}{d_{inj}} \right)^{-2/3} \tag{14}$$

The mean mixture fraction is assumed to be 1 in the injected gas stream (pure fuel) and 0 in the cross flow (pure oxidizer):

$$m = \frac{W_{inj}}{W} \tag{15}$$

$$\tilde{f}_{CL} = \frac{C_{CL} m}{1 + (m - 1) C_{CL}} \tag{16}$$

$$\tilde{f}(s, n) = \tilde{f}_{CL} \exp \left(\frac{-n^2}{2b} \right) \tag{17}$$

The mixture fraction at a given point is determined by the centerline mixture fraction corresponding to that point, and by the jet spreading distance, which is a function of distance from the injector along jet centerline.

$$n^2 = (x - x_{CL})^2 + (y - y_{CL})^2 + z^2 \tag{18}$$

$$\frac{b}{d_{inj}} = c_4 r_u^{2/3} \left(\frac{x_{CL}}{d_{inj}} \right)^{1/3} \tag{19}$$

Thus, by computing the shortest perpendicular distance from a given point to the jet centerline, the mixture fraction can be computed. The constants c_1-c_5 are experimentally determined. Their values in MASIV are given in Table 4.

The mean mixture fraction variance is computed by another scaling argument. Measurements indicate that mixture fraction variance is essentially a function of rate of change of mean mixture fraction, so that

$$\widetilde{f'} = c_5 \frac{\partial f}{\partial r} \tag{20}$$

$$\widetilde{f'} = c_5 \frac{r}{b} f \tag{21}$$

American Institute of Aeronautics and Astronautics

Table 4. Experimental constants for jet mixing model.

Constant	Experimental Range	MASIV value
c_1	1.2 to 2.6[10]	2.1
c_2	0.28 to 0.34[10]	$\frac{1}{3}$
c_3	0.85-0.95[11]	0.9
c_4	0.35[5]	0.35
c_5	0.14	0.14

Finally, we determine the local scalar dissipation rate, $\widetilde{\chi}$ using the formula:

$$\chi = 2D|\nabla f|^2 \tag{22}$$

$$\widetilde{\chi} = 2D_T|\nabla \tilde{f}|^2 \tag{23}$$

where D is the scalar diffusion coefficient and D_T is the turbulent scalar diffusion coefficient. We can estimate D_T using[12]

$$\frac{u_0 d}{\nu_T} \approx 65 \tag{24}$$

$$\mathrm{Sc}_T = \frac{\nu_T}{D_T} \tag{25}$$

$$\approx 0.55 \tag{26}$$

D.   Solution Procedure

To solve for combustion in the duct, we first define a geometry $(A, \frac{dA}{dx})$ and a fuel injection profile $(\frac{d\dot{m}}{dx})$ as functions of axial distance, x. For a given fuel injection location, we know the mass flow rate of fuel that enters the duct. Based on the fuel mass flow rate, the jet scaling law gives us a 3-dimensional flow field in which

$$\tilde{f} = \tilde{f}(x, y, z) \tag{27}$$

$$\widetilde{f'} = \widetilde{f'}(x, y, z) \tag{28}$$

$$\widetilde{\chi} = \widetilde{\chi}(x, y, z) \tag{29}$$

$$\widetilde{\omega}_i = \widetilde{\omega}_i(\tilde{f}, \widetilde{f'}, \widetilde{\chi}) \tag{30}$$

$$\widetilde{\omega}_i = \widetilde{\omega}_i(x, y, z) \tag{31}$$

We then integrate $\dot{\omega}(x, y, z)$ to determine the 1-dimensional rate of reaction of each species:

$$\widetilde{\omega}_i(x) = \iint \widetilde{\omega}_i(x, y, z) dy\, dz \tag{32}$$

With $\dot{\omega}(x)$ we now have enough information to solve the equations in Table 2. A stiff solver is required, due to the rapid reaction rates. We used MATLAB's `ode23tb`.

IV.   Comparison to Experiment

Experiments were performed in the supersonic combustion facility at the University of Michigan. This facility supplies 21mole fraction vitiated air with stagnation temperatures (T_0) up 1500 K. The test section is made of stainless steel and is shown in Figure 1. A two-dimensional Mach 2.2 nozzle exits into a constant area isolator with a cross section of 25.4 mm by 38.1 mm. The constant-area isolator is followed by a wall cavity flameholder and a nozzle section with a 4 degree divergence angle. Room temperature gaseous fuel

American Institute of Aeronautics and Astronautics

was injected sonically through a single 2.49 mm diameter port located on the test section centerline 44.5 mm upstream of the cavity leading edge. Pilot fuel was also injected through three ports in the cavity trailing edge. Additional details on the facility and test section can be found in Reference [13].

Wall static pressure ports were located throughout the combustor and isolator with a spacing of 25.4 mm to 38.1 mm. During each run, pressure data was recorded at eight locations at 40 Hz. For two runs, the monitoring locations were changed between runs to obtain the average pressure at 30 locations the test section.

Estimates of the heat release distribution in the combustor where acquired using images of the OH* luminosity.[14] Chemiluminescence is often used as a marker of the heat release in flames,[15–17] and OH* is individually proportional to the heat release rate in many cases.[18] The luminosity from OH* was imaged using a Andor Istar intensified camera with a 310±10 nm bandpass interference filter. Previous measurements made in this combustor with a mixture of ethylene and hydrogen fuel showed little difference between the OH* and CH* signals.[14] Thus the contribution of OH* from the hot products appears to minor compared to the contribution of OH* in the reaction zone.
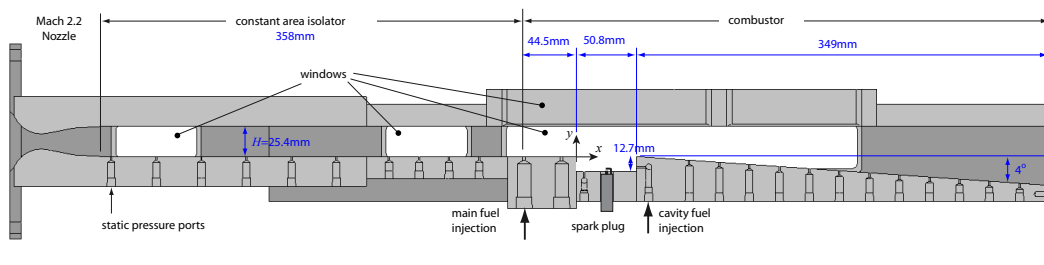

Figure 7. University of Michigan dual-mode combustor.

A. Experimental Run Details

Table 5. Run conditions for the experiment.

T_0	p_0	T	p	fuel composition	oxidizer composition	ϕ
1300 K	339300 Pa	1216 K	260900 Pa	$Y_{H_2} = 1$	$Y_{O_2} = 0.249$ $Y_{N_2} = 0.629$ $Y_{H_2O} = 0.123$	0.27

B. MASIV Run Details

The duct used to represent the combustion experiment in MASIV is shown in Figure 8. The current results simulate the combustor section of the duct, stations 4a to 4b. Note that these results are produced without any tuning of the system for this specific case. The constants used are presented in Table 6.

Table 6. Constant parameters used in the simulation.

Parameter	Value
Pr	0.71
T_w	1100 K
C_f	0.003

While it would be possible to obtain better agreement with the experiment by tailoring the input to the simulation to match the experimental results, this effort aims to represent ducts using generic constants, such that results will be extensible. We sacrifice accuracy for particular cases in an attempt to develop scaling laws useful for a wider range of configurations. Figure 9 compares the MASIV result to the experimental
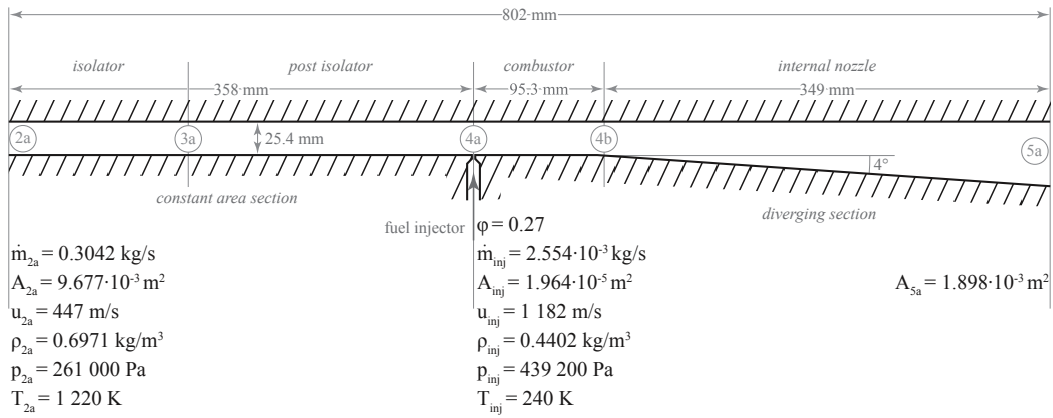
American Institute of Aeronautics and Astronautics

Figure 8. Simplified duct geometry for simulation.

result. The evolutions of the other thermodynamic quantities, for which there are no experimental data, are presented in Figure 10.

Although the computational result shows strong similarity to the experiment in its curvature, there are clearly several differences. First, the computed curve drops more sharply around the fuel injection point, which could be due to the simplicity of the mixing model, which assumes that the mass of each species is uniformly distributed within each cross section. That is, injected mass is assumed to mix rapidly into the main flow.

No experimental data were available for the temperature of the duct walls or wall friction, which has a strong effect on the result. Cold walls can remove a great deal of enthalpy from the flow, as can friction work. Experience suggests that the walls of the experiment will be slightly cooler than the vitiated air stagnation temperature, since they will not have enough time to reach equilibrium with the flow. Friction is estimated using Van Driest's relation.[19]

Confinement has an effect on the centerline penetration and spreading of the jet, which is not included in the scaling relations of Hasselbrink and Mungal. Experimental results suggest that the walls may prevent the jet from penetrating as far as it would otherwise, but the effect on the heat release distribution is unclear. The cavity also has an effect on the area of the flow, but this effect is not modeled here.

V.   Conclusions

The MASIV code computes duct solutions for arbitrary duct configurations for use in control design and evaluation. The solutions require about 30 seconds for a typical run and they include a modern

Results from the inlet solver are compared to correspond CFD results. The inlet model results give good agreement, and less smearing than the CFD solution for inviscid cases.

Results from the combustion duct solver are compared to the pressure results of an experimental setup which is applicable to hypersonic vehicle engine analysis, the dual-mode (ram/scramjet) combustor at the University of Michigan. Simulation results show good similarity to experiment, with no "tuning" of the parameters used in the code. Instead, the constants were selected from previous experimental studies.

Acknowledgements

References

[1]Torrez, S. M.; Scholten, N. M. D. D. J. F. B. M. D. D. and Oppenheimer, M. W., "A Scramjet Engine Model Including Effects of Precombustion Shocks and Dissociation," AIAA 2008-4619.

[2]Torrez, S. M. Driscoll, J. F. B. M. A. O. M. W. and Doman, D., "Effects of Improved Propulsion Modelling on the Flight
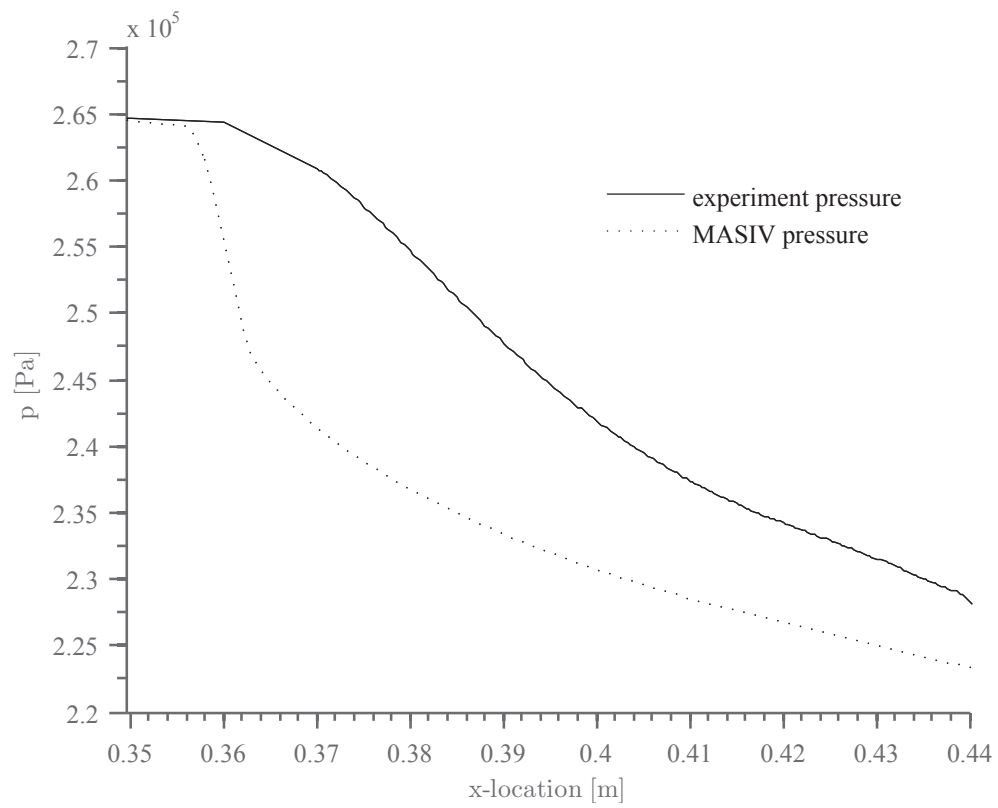
American Institute of Aeronautics and Astronautics

Figure 9. Comparison of computed and measured pressures.

American Institute of Aeronautics and Astronautics

a) axial velocity

b) Mach number

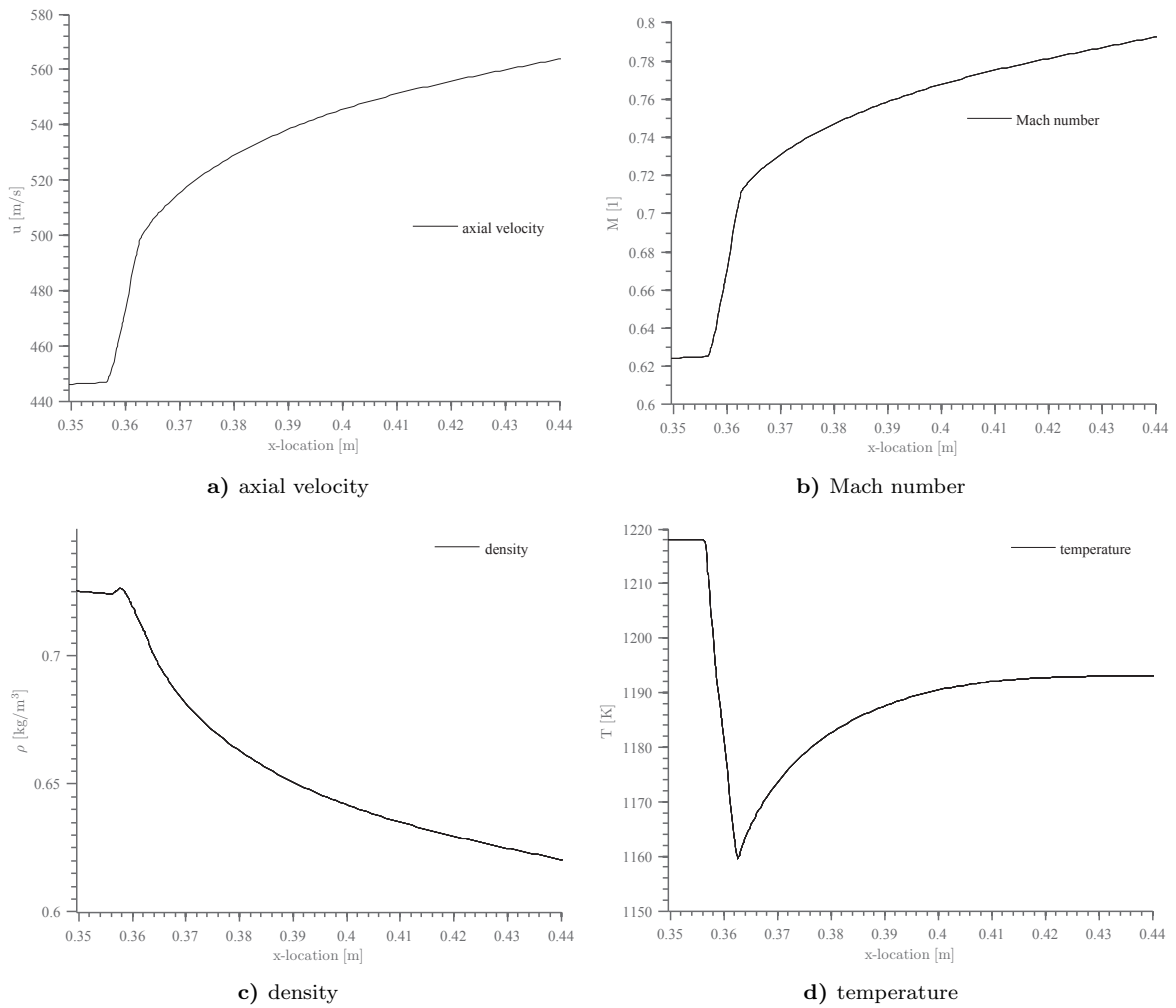**c)** density

d) temperature

Figure 10. The evolutions of p, T, u, M in the axial direction, computed by MASIV.

Dynamics of Hypersonic Vehicle," 2008.

[3]Anderson, J. D., *Modern Compressible Flow*, McGraw Hill, 3rd ed., 2003.

[4]O'Brien, T. F.; Starkey, R. P. and Lewis, M. J., "Quasi-One-Dimensional High-Speed Engine Model with Finite-Rate Chemistry," *Journal of Propulsion and Power*, Vol. Vol. 17, No. 6, 2001, pp. pp. 1366–1374.

[5]Hasselbrink, E. F. and Mungal, M. G., "Transverse jets and jet flames. Part 2. Velocity and OH field imaging," *Journal of Fluid Mechanics*, Vol. 443, 2001, pp. 27–68.

[6]Peters, N., "Laminar Diffusion Flamelet Models in Non-Premixed Turbulent Combustion," *Progress in Energy Combustion Science*, Vol. 10, 1984, pp. 319–339.

[7]R. J. Kee, F. M. Rupley, J. A. M. M. E. C. J. F. G. E. M. H. K. M. A. E. L. G. D.-L. M. D. S. J. W. G. H. E. R. S. L. R. E. M. L. R. P. W. C. R. M. C. W. E. S. P. G. C. W. C. L. M. O. A. W. G. H. C. P. C. S. F. M. P. H. P. D. Y. D. J. Y. D. W. H. M. V. P. and Puduppakkam, K. V., *CHEMKIN Release 4.1*, Reaction Design, San Diego, CA, 2006.

[8]Heiser, W. and D., P., *Hypersonic Airbreathing Propulsion*, American Institute of Aeronautics and Astronautics, 370 L'Enfant Promenade, SW,Washington D.C., 20024-2518, 1994, pp. 109–143.

[9]Pitsch, H., "FlameMaster v3.1: A C++ computer program for 0D combustion and 1D laminar flame calculations." 1998.

[10]Hasselbrink, E. F. and Mungal, M. G., "Transverse Jets and Jet Flames: Part 1. Scaling Laws for Strong Transverse Jets," *Journal of Fluid Mechanics*, Vol. Vol. 443, 2001, pp. pp. 1–25.

[11]Smith, S. H. and Mungal, M. G., "Mixing, structure and scaling of the jet in crossflow," *Journal of Fluid Mechanics*, Vol. 357, 1998, pp. 83–122.

[12]Peters, N., "Die Struktur turbulenter Freistrahl-Diffusionsflammen," *Chemie Ingenieur Technik*, Vol. 55 No. 10, 1983, pp. 743–751.

[13]Micka, D. J. and Driscoll, J. F., "Combustion characteristics of a dual-mode scramjet combustor with cavity flameholder," *Proc. Comb. Inst.*, Vol. 32, 2009, pp. 2397–2404.

[14]Micka, D. J., Torrez, S. M., and Driscoll, J. F., "Measurements and Modeling of the Heat Release Distribution in a Dual-mode Scramjet Combustor with Wall Fuel Injection," *Proceedings of the 6th U.S. National Combustion Meeting*, 2009.

[15]Price, R. B., Hule, I. R., and Sugden, T. M., "Optical studies of the generation of noise in turbulent flames," *Proc. Comb. Inst.*, Vol. 12, 1968, pp. 1093–1102.

[16]Najm, H. N., Paul, P. H., Mueller, C. J., and Wycokoff, P. S., "On the adequacy of certain experimental observables as measurements of flame burning rate," *Combust. Flame*, Vol. 113, 1998, pp. 312–332.

[17]Meier, W., Weigand, P., Duan, X., and Giezendanner-Thoben, R., "Detailed characterization of the dynamics of thermoacoustic pulsations in a lean premixed swirl flame," *Combust. Flame*, Vol. 150, 2007, pp. 2–26.

[18]Hardalupas, Y. and Orain, M., "Local measurements of the time-dependent heat release rate and equivalence ratio using chemiluminescent emmission from a flame," *Combust. Flame*, Vol. 139, 2004, pp. 188–2007.

[19]White, F. M., *Viscous Fluid Flow*, McGraw Hill, 3rd ed., 2006.

American Institute of Aeronautics and Astronautics